Journal of Hazardous Materials 173 (2010) 265–272

Contents lists available at ScienceDirect

Journal of Hazardous Materials

journal homepage: www.elsevier.com/locate/jhazmat

Effects of europium doping on the photocatalytic behavior of $BiVO_4$

Aiping Zhang*, Jinzhi Zhang

College of Sciences, North China University of Technology, Beijing 100144, PR China

ARTICLE INFO

Article history:
Received 17 June 2009
Received in revised form 17 August 2009
Accepted 18 August 2009
Available online 25 August 2009

Keywords:
Photocatalyst
$Eu/BiVO_4$ composite
Visible light

ABSTRACT

$Eu/BiVO_4$ composite photocatalysts have been hydrothermally synthesized and characterized by XRD, XPS, SEM, EDS and DRS techniques. The photocatalytic activities of these catalysts were evaluated by the decolorization of methyl orange in aqueous solution under visible light irradiation ($\lambda > 420$ nm). It proved that the enhanced activities of $Eu/BiVO_4$ composites are mainly ascribed to the dopants for the effective electron–hole separation effect, and the optimum content of the doped metal can be controlled by adjusting the ratio of the rare materials in precursor.

1. Introduction

Bismuth vanadate ($BiVO_4$) has recently attracted considerable attention not only for its interesting technological properties [1,2], but also for its strong photocatalytic effect on water splitting and organic pollutant decomposing under visible light irradiation [3–7]. However, the low photocatalytic activity of pure $BiVO_4$ restricts its widely application to the photocatalytic degradation of organic contaminants. Then the modification technology of metal doping has been used to enhance the activity of $BiVO_4$. To date, Fe [8], Co [8–10], Cu [9,11,12], Pd [13,14], Mn [15], Ag [16–18], Ce [19], W [20], Mo [21], V [22], Bi [23] and other metals doped in $BiVO_4$ have been demonstrated to be effective in the enhancement of their photocatalytic activities. Therefore, $BiVO_4$ doped with metal ions or metal oxides is considered to be a feasible route for enhancing the photodegradation of organic contaminants.

Although there have been many reports on transition metal and noble metal doped in $BiVO_4$, the effect of rare earth element doping on the photocatalytic activity of $BiVO_4$ for the organic contaminants photodegradation has seldom been reported so far as we know. However, other investigations showed that lanthanide ions/oxides with 4f electron configuration were better dopants in photocatalysts. El-Bahy et al. [24] reported that lanthanide ions (La^{3+}, Nd^{3+}, Sm^{3+}, Eu^{3+}, Gd^{3+} and Yb^{3+}) doped TiO_2 were synthesized by sol–gel method, and lanthanide ions can enhance the photocatalytic activity of TiO_2 for photodegradation of direct blue. Xie et al. [25] reported that doping with Eu^{3+}, Nd^{3+} and Ce^{4+} increased the photocatalytic activities of TiO_2 catalysts in aqueous azo dye (X-3B) solution under visible light irradiation. Therefore, using lanthanide element doped in catalysts could be an efficient way to increase the photocatalytic activity.

In this work, $BiVO_4$ was doped with different content of europium (Eu) and characterized by XRD, XPS, SEM, EDS and DRS techniques. The influence of Eu doping on the photocatalytic decolorization of methyl orange was studied under visible light irradiation. The proposed mechanism of the improved activity in $Eu/BiVO_4$ composites was also discussed.

2. Experimental

2.1. Synthesis of $Eu/BiVO_4$ composite catalysts

In a typical hydrothermal processing, 0.02 mol $Bi(NO_3)_3{\cdot}5H_2O$ and 0.02 mol NH_4VO_3 were dissolved separately in 20 mL of 35% (w/w) HNO_3 and 20 mL of 6 mol/L NaOH solutions, and each stirred for 30 min at room temperature (RT). After that, these two mixtures were mixed together in 1:1 molar ratio and stirred for about 30 min to get a stable, salmon pink homogeneous solution. The different amounts of $Eu(NO_3)_3$ (0.1, 0.2, 0.5, 1.0 and 2.0 g) were then added into these solutions individually with a continuing stirring for 30 min to get the precursors. Mixture of each precursor were then sealed in a 50 mL Teflon-lined stainless autoclave and heated to 180 °C for 6 h under autogenous pressure. Afterwards, the precipitate was filtered, washed with distilled water three times for each, and dried in vacuum at RT for 12 h.

2.2. Apparatus and measurements

X-ray powder diffraction patterns (XRD, Puxi Co. LTD, model XD-3) were recorded in the region of $2\theta = 17–55°$ using Cu Kα

* Corresponding author. Tel.: +86 10 88803271; fax: +86 10 88803271.
E-mail address: ncutalex@126.com (A. Zhang).

0304-3894/$ – see front matter © 2009 Elsevier B.V. All rights reserved.
doi:10.1016/j.jhazmat.2009.08.079

radiation with a scan step of 2.0°/min at RT using a counter diffractometer. The morphologies and microstructures of as-prepared samples were examined with scanning electron microscopy (SEM, FEI Co., model Quanta-600). Energy dispersive spectrometry (EDS) used with SEM was also taken for the chemical analysis of the samples. Optical absorption spectra were obtained on a double-beam UV–vis spectrophotometer (Puxi Co. LTD, model TU-1901) equipped with an integrating sphere. UV–vis diffuse reflectance spectra (DRS) of $BiVO_4$ were recorded using $BaSO_4$ as a reference and were converted from reflection to absorbance by Kubelka–Munk method from its equipped software. X-ray photoelectron spectroscopy (XPS) analysis was performed on a VG MKII X-ray photoelectron spectrometer using the Mg Kα radiation.

2.3. Photocatalytic activity test

Photocatalytic activities of the samples were determined by the decolorization of methyl orange (MO) under a visible light irradiation. A 500 W Xe-illuminator was used as a light source and set about 10 cm apart from the reactor. The 420 nm cut-off filter was placed between the Xe-illuminator and the reactor to completely remove all incoming wavelengths shorter than 420 nm to provide visible light ($\lambda > 420$ nm). Experiments were carried out at ambient temperature as follows: the same amount (0.2 g) of photocatalyst was added into 100 mL of 10 mg/L MO solution. Before illumination, the solutions were stirred for 30 min in dark in order to reach the adsorption–desorption equilibrium for MO and dissolved oxygen. At different irradiation time intervals, about 5 mL suspensions were collected, and centrifugalized to remove the photocatalyst particles. Then the concentrations of the remnant MO were monitored by checking the absorption spectrum of each sample.

3. Results and discussion

3.1. Powder formation

Fig. 1A shows the XRD diffraction patterns of the pure $BiVO_4$ and Eu/$BiVO_4$ series photocatalysts. It is confirmed that all the photocatalysts have a single monoclinic-scheelite structure, and no signal for any other phases about europium or impurities can be detected in the composite samples for their low content of Eu element. The diffraction peaks of all samples are in conformity to the standard card of monoclinic $BiVO_4$ (JCPDS cards No.: 14-0688). Fig. 1B portrays the shift of the peaks at about 28.9 and 30.5° corresponded to the (1 2 1) and (0 4 0) planes, respectively. There is a gradual shift in these peaks toward right with the increase of Eu content, suggesting that the increased Eu dopant in the composites lead to a tiny change in their local crystal structures by degrees.

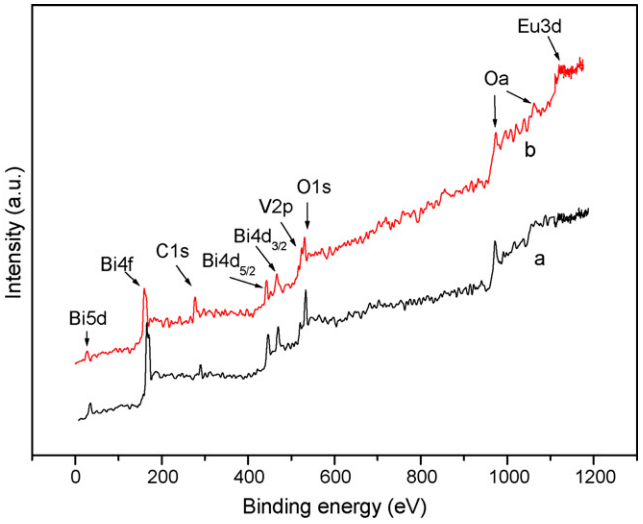

Fig. 2. XPS of (a) pure $BiVO_4$ crystallites and (b) 1.46 wt% Eu/$BiVO_4$ composite photocatalysts.

The overall XPS spectra for the pure $BiVO_4$ crystallites and Eu/$BiVO_4$ composite photocatalysts are shown in Fig. 2. It is indicated that the Eu 3d peak around 1120 eV can be detected obscurely for the Eu/$BiVO_4$ composite compared with the pure $BiVO_4$. Fig. 3 shows high-resolution XPS spectra of the four primary elements in the composite. As is shown, the binding energies of Bi $4f_{7/2}$, Bi $4f_{5/2}$, V $2p_{3/2}$, V $2p_{1/2}$ and O 1s are 159.2, 164.3, 516.9, 529.9 and 529.8 eV,

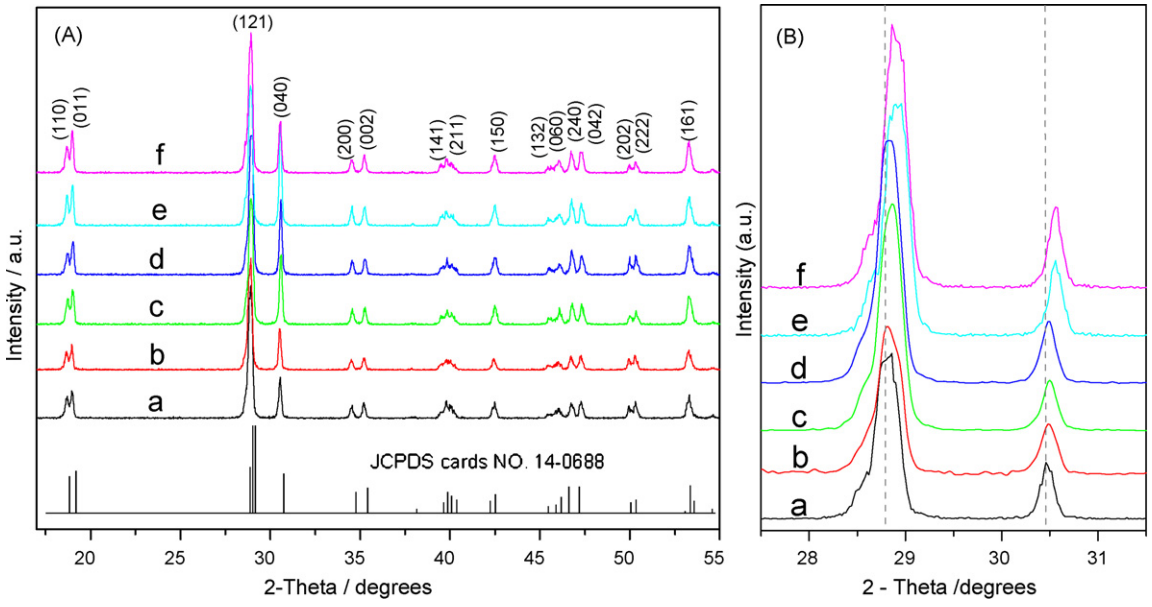

Fig. 1. (A) XRD patterns and (B) XRD peaks in (1 2 1) and (0 4 0) planes of different catalysts: (a) pure $BiVO_4$, (b) 0.36 wt% Eu/$BiVO_4$, (c) 0.73 wt% Eu/$BiVO_4$, (d) 1.46 wt% Eu/$BiVO_4$, (e) 3.65 wt% Eu/$BiVO_4$ and (f) 7.30 wt% Eu/$BiVO_4$.

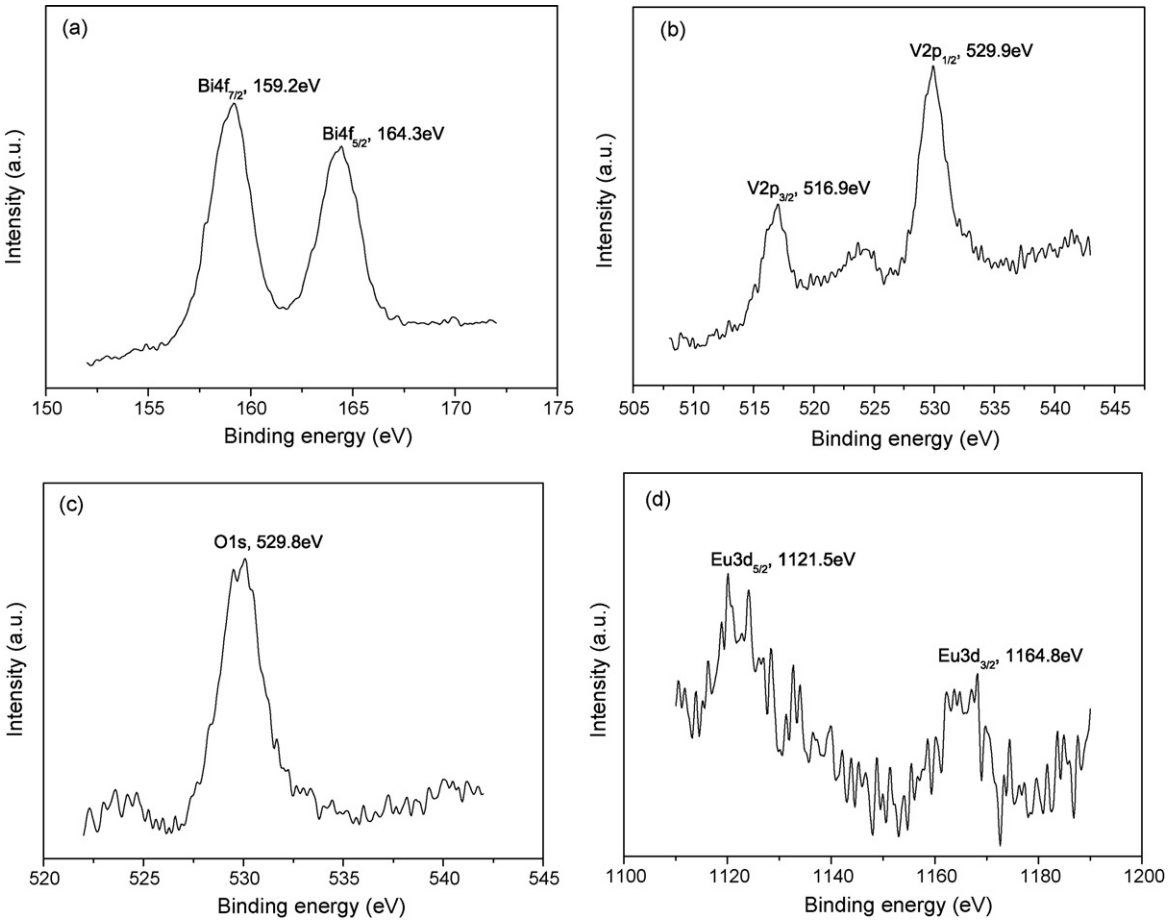

Fig. 3. XPS analysis of 1.46 wt% Eu/$BiVO_4$ composite photocatalysts: (a) Bi 4f; (b) V 2p; (c) O 1s; (d) Eu 3d.

respectively. The Eu 3d region (Fig. 3d) is displayed with the characteristic peaks at 1121.5 and 1164.8 eV, ascribed to Eu $3d_{5/2}$ and Eu $3d_{3/2}$ respectively; and it has a 43 eV splitting of the Eu 3d doublets, which is a character of Eu^{3+} anion and consistent with those of Eu in the form of Eu_2O_3 [26,27].

3.2. Morphologies and structures performance

The SEM images of different catalysts are shown in Fig. 4. The primary particle of the pure $BiVO_4$ had a spherical shape generally (Fig. 4a), and sintered with each other strongly to be a large cluster. From Fig. 4b to f, it is clear seen that with the increase of Eu content, the dispersive particles with few clusters and some larger crystals with smooth surface and edged shape came into being. This can signify that the presence of Eu in the reaction media may influence the formation of particles via a characteristic nucleation–dissolution–recrystallization effect in the processing [28].

The chemical composition of each sample was determined using EDS technique. Fig. 5 shows the average EDS signals obtained from measuring a large scale (100 times of the whole SEM images area) of each sample. Besides the obvious signals for O, Bi and V elements marked in Fig. 5a, the EDS spectra shows that very weak signal of europium with an increasing trend was detected in the Eu/$BiVO_4$ composites. And the obtained amount of dopant from EDS analysis is in good agreement with the doping contents calculated from the rare precursor, as listed in Table 1.

The UV–vis diffuse reflectance spectra (DRS) spectra of Eu/$BiVO_4$ composites in comparison with pure $BiVO_4$ are shown in Fig. 6. For the pure $BiVO_4$, a steep absorption edge near 550 nm can be attributed to the band-gap excitation of monoclinic $BiVO_4$; and it shows no light absorption above 650 nm. Whereas, Eu-doped $BiVO_4$ samples exhibit red-shift of their absorption edges and significant enhancement of absorption in the region $\lambda > 650$ nm. According to the EDS and XRD results, the presence of Eu dopant in $BiVO_4$ does not modify their crystal type and the corresponding band edges. Instead, it may introduce new energy levels of the dopants into the band-gap of $BiVO_4$. Therefore, the absorption edges, shifting toward longer wavelengths for the composites, may come from the electronic transition from the dopant energy level to the energy bands of $BiVO_4$. Additionally, a newly appeared band centered at ca. 780 nm, may be introduced by the f-f transition of Eu^{3+} anion or the charge transfer transition between interacting ions.

3.3. Photocatalytic activities of the catalysts

3.3.1. UV–vis absorption spectra changes

The changes in the absorption spectra of methyl orange (MO) aqueous solutions during the photodegradation process by the pure and Eu-doped $BiVO_4$ at different irradiation time are shown in Fig. 7. Before irradiation, it shows two distinctive bands centered at 465 and 270 nm for MO solution. And the 465 nm band of MO in the visible region is meaningful with respect to the nitrogen-to-nitrogen double bond (–N=N–) of the azo dye, as the most active site for oxidative attack. Thus, the decrease of absorption bands at $\lambda_{max} = 465$ nm is always used to indicate the degradation of MO molecules.

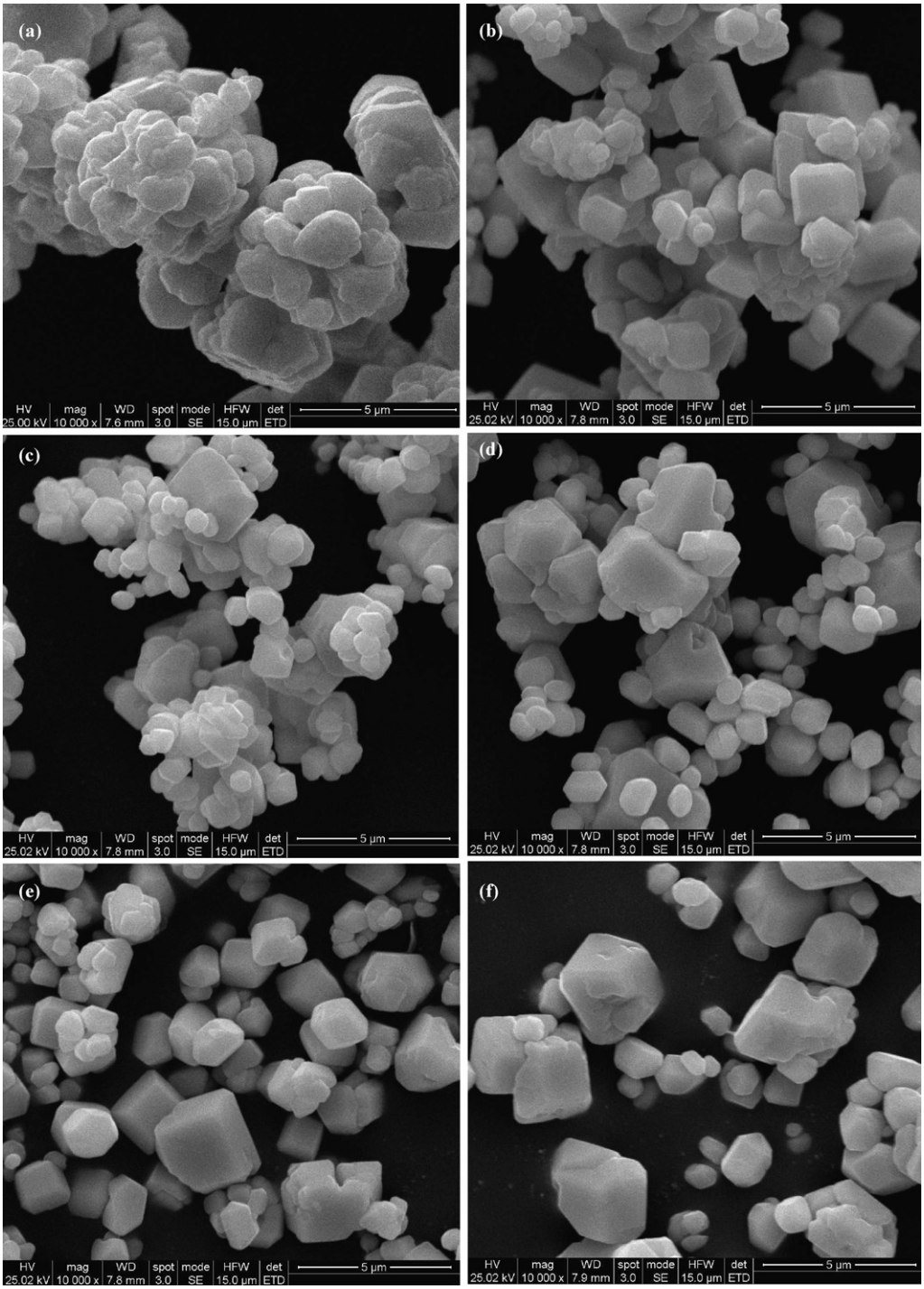

Fig. 4. SEM images of (a) pure $BiVO_4$, (b) 0.36 wt% $Eu/BiVO_4$, (c) 0.73 wt% $Eu/BiVO_4$, (d) 1.46 wt% $Eu/BiVO_4$, (e) 3.65 wt% $Eu/BiVO_4$ and (f) 7.30 wt% $Eu/BiVO_4$.

3.3.2. Effects of Eu doping on photodegradation of MO molecules

The photodegradation rate of MO on $Eu/BiVO_4$ composite catalysts compared with that of pure $BiVO_4$ under visible light irradiation within 180 min are shown in Fig. 8A. For the pure $BiVO_4$, the absorbance of MO at 465 nm slowly decreased to 0.764 after 180 min irradiation, and the total photodegradation rate of MO was 13.7%, which means that only a little part of the MO molecules in the solution had been decomposed. When using the composites with a Eu content of 0.36, 0.73, 1.46, 3.65 and 7.30 wt%, the photodegradation rates of MO had promptly reached to 54.8, 50.7, 89.8, 72.4 and 41.9% after irradiating only 90 min and reached up to 85.8, 89.9, 93.6, 89.6 and 65.2% after irradiating 180 min, which shows much higher than that of pure $BiVO_4$. Though the photocatalytic activity of $Eu/BiVO_4$ composite was improved compared with pure $BiVO_4$, the enhanced activity of these composites did not increase further for those with more Eu in the content above 1.46 wt%. As shown in Fig. 8A, for the composites with 3.65 and 7.30 wt% europium, their total photodegradation rates of MO after 180 min irradiation were lower compared with the sample with 1.46 wt% europium. In addition, the adsorption rate of the 10 mg/L MO over pure and $Eu/BiVO_4$ catalysts are also shown in Fig. 8A. After a continuing stirring for 30 min in darkness to reach the adsorption–desorption equilibrium, the adsorption rate were 5.4, 8.7, 6.3, 10.1, 9.2 and 8.5% for the pure $BiVO_4$, the 0.36, 0.73, 1.46, 3.65 and 7.30 wt% $Eu/BiVO_4$

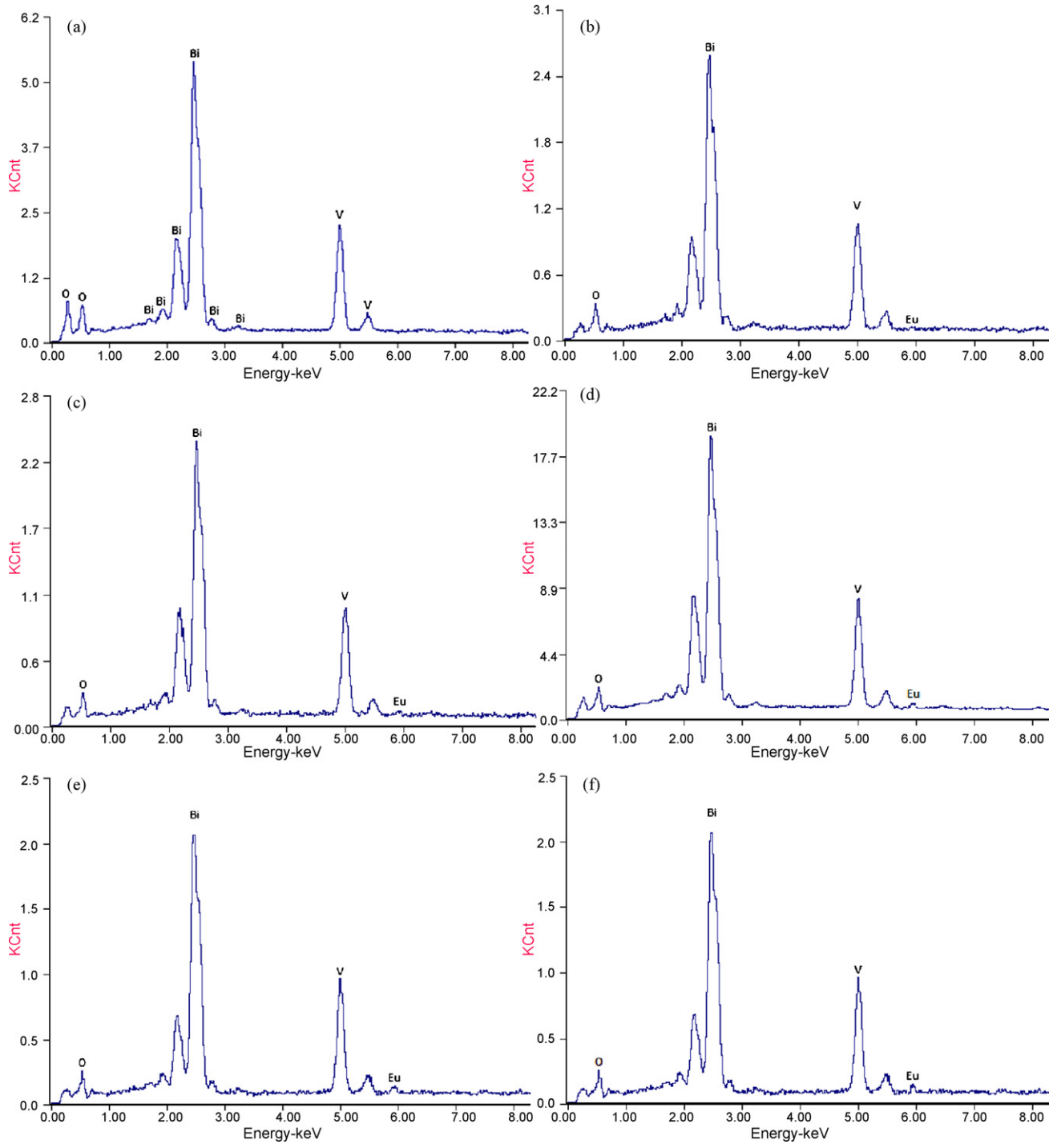

Fig. 5. EDS results of (a) pure $BiVO_4$, (b) 0.36 wt% Eu/$BiVO_4$, (c) 0.73 wt% Eu/$BiVO_4$, (d) 1.46 wt% Eu/$BiVO_4$, (e) 3.65 wt% Eu/$BiVO_4$ and (f) 7.30 wt% Eu/$BiVO_4$.

composites, respectively. Although the photocatalytic activities of these composites were much high, the adsorption rate of all these catalysts were close to each other. Thus, the high adsorption ability of these catalysts is supposed to be only one of the reasons for the enhanced decomposition of MO dye molecules.

3.3.3. *Kinetics of photocatalytic degradation of MO molecules*

Most of the heterogeneous photocatalytic degradation reactions follow Langmuir–Hinshelwood kinetic [29] $\ln(C_0/C_t) = kt + a$, where k is the apparent reaction rate constant, C_0 is the initial concentration, C_t is the concentration at the reaction time of t, and t is the reaction time. As is known, the concentration (C) of MO has a lin-

Table 1
Europium content in the catalysts by theoretical and EDS experiments.

Samples	Theoretical (wt%)	Experimental (wt%)
Pure $BiVO_4$	0.00	0.00
Eu/$BiVO_4$ composite	0.36	0.32
Eu/$BiVO_4$ composite	0.73	0.69
Eu/$BiVO_4$ composite	1.46	1.28
Eu/$BiVO_4$ composite	3.56	3.22
Eu/$BiVO_4$ composite	7.30	6.58

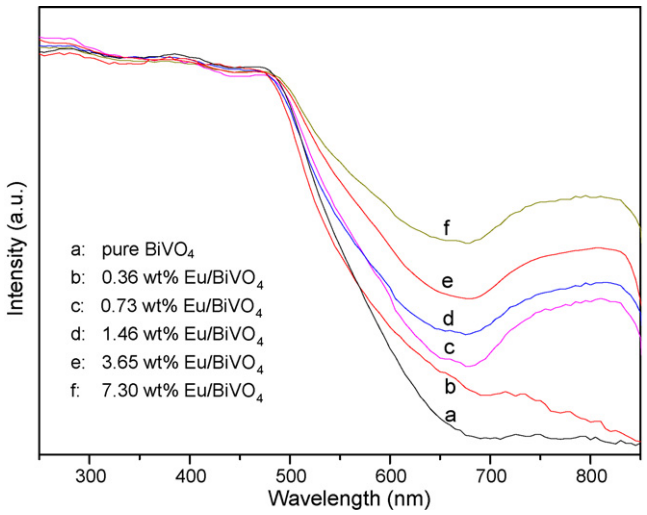

Fig. 6. UV–vis diffuses reflectance spectra of pure and Eu/$BiVO_4$ series catalysts.

ear relation with the absorbance (A), thus, $\ln(C_0/C_t) = \ln(A_0/A_t)$; and the above can be approximated to $\ln(A_0/A_t) = kt + a$, which belong to the first-order kinetics. This is confirmed by a nearly linear plot of $\ln(C_0/C_t)$ with t, as shown in Fig. 8B. And the kinetic parameters for each catalyst can be calculated and have listed in the inset table of Fig. 8B.

3.3.4. *Effects of Eu dopant on the activity of $BiVO_4$ catalysts*

The increased activity of catalyst was proposed to occur via the trapping of photogenerated electrons in the catalyst by Eu dopant, thereby reducing the extent of deleterious electron–hole recombination [30,31]. From the DRS results, it indicated that the Eu doping lead to the enhanced absorbance and a new absorption band in the visible light region. That is to say, the doped europium may provide a shallow trap for photogenerated electron and hole so as to inhibit the recombination and extend the lifetime of charge carrier. Therefore, the photodegradation rate could be enhanced consequently because more charge carriers are available. Yang et al. [32] thought dye molecules interact simultaneously with the dopant and main

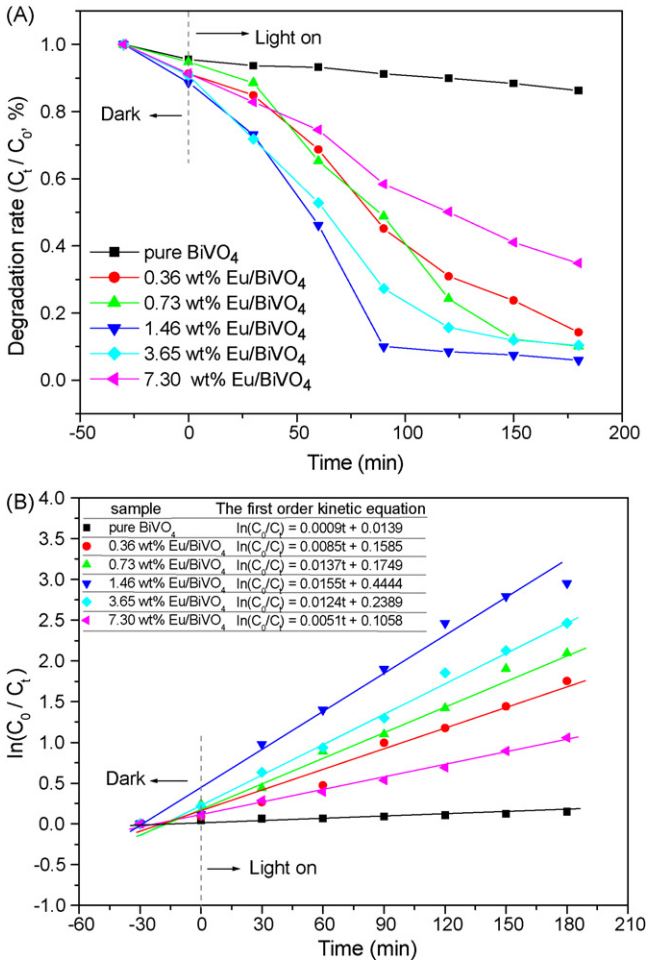

Fig. 8. The degradation rate (A) and relationship (B) between $\ln(C_0/C_t)$ and treatment time of as-prepared catalysts.

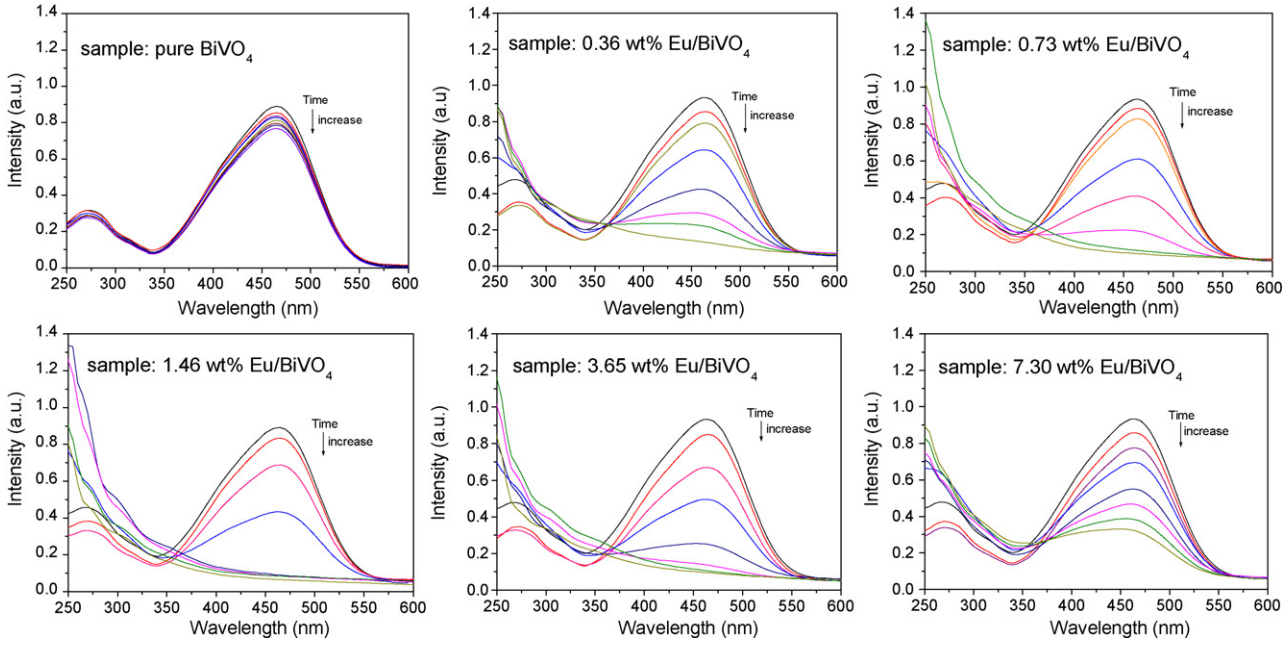

Fig. 7. UV–vis absorption spectra profile changes of photocatalytic degradation of 10 mg/L MO by pure and series Eu-doped $BiVO_4$ catalysts at different irradiation times.

component yielding an intermediate species, which play an important role in the photocatalytic degradation mechanism or Eu oxides, may act as receptors or transmitters of the photogenerated electrons. Xu et al. [33] suggested that a Eu^{3+} ion has an unfilled 4f shell and the reduction of Eu^{3+} is thermodynamically feasible, it is valid to assume that electron can be trapped by Eu^{3+} on the surface of catalyst. As a result of the electron trapping by Eu^{3+}, the rate of the electron–hole recombination reaction is slowed down and more holes are available for the redox reactions. Wu et al. [34] also reported that surface electrons can be trapped by the Eu^{3+} ion to form a reduction species Eu^{2+} ion; and if oxygen is present in the system, the Eu^{2+} could be oxidized back to Eu^{3+}. As a result of the recycle reactions, the electron hole recombination rate could be reduced.

However, these explanations seem to explain the enhancement at low Eu content but do not account for the negative effect observed with further increasing the Eu content. As shown in Fig. 8A, the 1.46 wt% Eu/$BiVO_4$ represented the highest activity, and the photodegradation rate of MO was found to decrease when using those with higher Eu content. A plausible explanation for this phenomenon may be due to the short-circuiting mechanism of the coupled reaction, which occurs only at Eu^{3+} content above a certain level. At high doping of europium, since the Eu^{3+} was confined on the surface of catalysts, there is a high possibility for the trapped electrons to recombine with the holes. The reduction of Eu^{3+} to Eu^{2+} by the photogenerated electrons is expected to be faster than the photocatalytic oxidation reaction by oxygen, since the former is simply a direct transfer of the trapped electron from Eu^{3+} to the valence band hole. In that case the excess Eu species may act as a recombination center or may cover the active sites on the $BiVO_4$ surface and thereby reduce the efficiency of charge separation.

4. Conclusion

The Eu/$BiVO_4$ composite photocatalysts were hydrothermal synthesized and characterized using many state-of-the-art techniques. XRD and SEM analysis showed that the Eu doping is good for the compounds to form monoclinic $BiVO_4$ structure and can influence the crystallinity of the compounds a little. The light absorption edges of Eu/$BiVO_4$ composites had extended a red-shift compared with that of pure $BiVO_4$. The low content of Eu doping can significantly increase the photocatalytic activity, however, the photocatalytic activity was found to decrease with the further increase of the Eu dopant. The photodegradation reactions of methyl orange by $BiVO_4$ and Eu-doped $BiVO_4$ follow the first-order kinetics. Thus, possible reasons for Eu/$BiVO_4$ composites showed higher activity than pure $BiVO_4$ are mostly in (1) the enhanced absorption in the visible region, (2) the suppressed recombination between photogenerated electrons and holes in composite samples, (3) the new absorption band corresponded to new energy levels and (4) the improved adsorption ability of dye molecules over the catalyst surfaces.

Acknowledgements

We acknowledge the financial support from the General Program of Beijing Municipal Education Committee (No. KM200910009011).

References

[1] A. Kudo, K. Omori, H. Kato, A novel aqueous process for preparation of crystal form-controlled and highly crystalline $BiVO_4$ powder from layered vanadates at room temperature and its photocatalytic and photophysical properties, J. Am. Chem. Soc. 121 (1999) 11459–11467.
[2] J.Q. Yu, A. Kudo, Effects of structural variation on the photocatalytic performance of hydrothermally synthesized $BiVO_4$, Adv. Funct. Mater. 16 (2006) 2163–2169.
[3] S. Kohtani, M. Koshiko, A. Kudo, K. Tokumura, Y. Ishigaki, A. Toriba, K. Hayakawa, R. Nakagaki, Photodegradation of 4-alkylphenols using $BiVO_4$ photocatalyst under irradiation with visible light from a solar simulator, Appl. Catal. B: Environ. 46 (2003) 573–586.
[4] A. Tücks, H.P. Beck, The photochromic effect of bismuth vanadate pigments: investigations on the photochromic mechanism, Dyes Pigments 72 (2007) 163–177.
[5] L. Zhang, D. Chen, X. Jiao, Monoclinic structured $BiVO_4$ nanosheets: hydrothermal preparation, formation mechanism, and coloristic and photocatalytic properties, J. Phys. Chem. B 110 (2006) 2668–2673.
[6] L. Zhou, W.Z. Wang, H.L. Xu, Controllable synthesis of three-dimensional well-defined $BiVO_4$ mesocrystals via a facile additive-free aqueous strategy, Cryst. Growth Des. 8 (2008) 728–733.
[7] A. Walsh, Y. Yan, M.N. Huda, M.M. Al-Jassim, S.H. Wei, Band edge electronic structure of $BiVO_4$: elucidating the role of the Bi s and V d orbitals, Chem. Mater. 21 (2009) 547–551.
[8] H. Xu, H. Li, C. Wu, J. Chu, Y. Yan, H. Shu, Preparation, characterization and photocatalytic activity of transition metal-loaded $BiVO_4$, Mater. Sci. Eng. B 147 (2008) 52–56.
[9] M. Guillodo, J. Fouletier, L. Dessemond, P.D. Gallo, Electrical properties of dense Me-doped bismuth vanadate (Me = Cu, Co) pO_2-dependent conductivity determined by impedance spectroscopy, J. Eur. Ceramic Soc. 21 (2001) 2331–2344.
[10] M. Long, W. Cai, J. Cai, B. Zhou, X. Chai, Y. Wu, Efficient photocatalytic degradation of phenol over Co_3O_4/$BiVO_4$ composite under visible light irradiation, J. Phys. Chem. B 110 (2006) 20211–20216.
[11] H. Xu, H. Li, C. Wu, J. Chu, Y. Yan, H. Shu, Z. Gu, Preparation, characterization and photocatalytic properties of Cu-loaded $BiVO_4$, J. Hazard. Mater. 153 (2008) 877–884.
[12] H. Jiang, H. Endo, H. Natori, M. Nagai, K. Kobayashi, Fabrication and efficient photocatalytic degradation of methylene blue over CuO/$BiVO_4$ composite under visible-light irradiation, Mater. Res. Bull. 44 (2009) 700–706.
[13] L. Ge, Novel Pd/$BiVO_4$ composite photocatalysts for efficient degradation of methyl orange under visible light irradiation, Mater. Chem. Phys. 107 (2008) 465–470.
[14] L. Ge, Synthesis and characterization of novel visible-light-driven Pd/$BiVO_4$ composite photocatalysts, Mater. Lett. 62 (2008) 926–928.
[15] Y.L. Yang, L. Qiu, W.T.A. Harrison, R. Christoffersen, A.J. Jacobson, Manganese-doped bismuth vanadate solid electrolytes. Part I: synthesis and characterisation of $Bi_2V_{1-x}Mn_xO_{5.5x}$, J. Mater. Chem. 7 (1997) 243–248.
[16] S. Kohtani, M. Tomohiro, K. Tokumura, R. Nakagaki, Photooxidation reactions of polycyclic aromatic hydrocarbons over pure and Ag-loaded $BiVO_4$ photocatalysts, Appl. Catal. B: Environ. 58 (2005) 265–272.
[17] K. Sayama, A. Nomura, T. Arai, T. Sugita, R. Abe, M. Yanagida, T. Oi, Y. Iwasaki, Y. Abe, H. Sugihara, Photoelectrochemical decomposition of water into H_2 and O_2 on porous $BiVO_4$ thin-film electrodes under visible light and significant effect of Ag ion treatment, J. Phys. Chem. B 110 (2006) 11352–11360.
[18] X. Zhang, Y. Zhang, X. Quan, S. Chen, Preparation of Ag doped $BiVO_4$ film and its enhanced photoelectrocatalytic (PEC) ability of phenol degradation under visible light, J. Hazard. Mater. doi:10.1016/j.jhazmat.2009.01.074.
[19] M.C. Neves, M. Lehocky, R. Soares, L. Lapcik, T. Trindade, Chemical bath deposition of cerium doped $BiVO_4$, Dyes Pigments 59 (2003) 181–184.
[20] P. Chatchai, Y. Murakami, S. Kishioka, A.Y. Nosaka, Y. Nosaka, Efficient photocatalytic activity of water oxidation over WO_3/$BiVO_4$ composite under visible light irradiation, Electrochim. Acta 54 (2009) 1147–1152.
[21] W. Yao, H. Iwai, J. Ye, Effects of molybdenum substitution on the photocatalytic behavior of $BiVO_4$, Dalton Trans. (2008) 1426–1430.
[22] H. Jiang, M. Nagai, K. Kobayashi, Enhanced photocatalytic activity for degradation of methylene blue over V_2O_5/$BiVO_4$ composite, J. Alloy Compd. 24 (2009) 821–827.
[23] L. Li, B. Yan, $BiVO_4$/Bi_2O_3 submicrometer sphere composite: microstructure and photocatalytic activity under visible-light irradiation, J. Alloy Compd. 476 (2008) 624–628.
[24] Z.M. El-Bahy, A.A. Ismail, R.M. Mohamed, Enhancement of titania by doping rare earth for photodegradation of organic dye (Direct Blue), J. Hazard. Mater. 166 (2009) 138–143.
[25] Y. Xie, C. Yuan, X. Li, Photosensitized and photocatalyzed degradation of azo dye using Ln^{n+}–TiO_2 sol in aqueous solution under visible light irradiation, Mater. Sci. Eng. B 117 (2005) 325–333.
[26] Y. Uwamino, T. Ishizuka, X-ray photoelectron spectroscopy of rare-earth compounds, J. Electron Spectrosc. Relat. Phenom. 34 (1984) 67–78.
[27] C.D. Wagner, D.A. Zatko, R.H. Raymond, Use of the oxygen KLL Auger lines in identification of surface chemical states by electron spectroscopy for chemical analysis, Anal. Chem. 52 (1980) 1445–1451.
[28] J.C. Sczancoski, M.D.R. Bomio, L.S. Cavalcante, M.R. Joya, P.S. Pizani, J.A. Varela, E. Longo, M.S. Li, J.A. Andres, Morphology and blue photoluminescence emission of $PbMoO_4$ processed in conventional hydrothermal, J. Phys. Chem. C 113 (2009) 5812–5822.
[29] D.F. Ollis, Contaminant degradation in water, Environ. Sci. Technol. 19 (1985) 480–484.
[30] E. Borgarello, J. Kiwi, M. Gratzel, E. Pelizzetti, M. Visca, Visible light induced water cleavage in colloidal solutions of chromium-doped titanium dioxide particles, J. Am. Chem. Soc. 104 (1982) 2996–3002.

[31] R.P. Saint-Arroman, J.M. Basset, F. Lefebvre, B. Didillon, Well-defined group IV supported catalysts: an efficient way to increase activities in the deperoxidation of cyclohexyl hydroperoxide with environmentally systems, Appl. Catal. A 285 (2005) 181–189.
[32] X. Yang, L. Xu, X. Yu, W. Li, K. Li, M. Huo, Y. Guo, Enhanced photocatalytic activity of Eu_2O_3/Ta_2O_5 mixed oxides on degradation of rhodamine B and 4-nitrophenol, Colloids Surf. A: Physicochem. Eng. Aspects 320 (2008) 61–67.
[33] J.J. Xu, Y.H. Ao, D.G. Fu, C.W. Yuan, A simple route for the preparation of Eu, N-codoped TiO_2 nanoparticles with enhanced visible light-induced photocatalytic activity, J. Colloid Interface Sci. 328 (2008) 447–451.
[34] X.H. Wu, W. Qin, X.B. Ding, W.D. He, Z.H. Jiang, Dopant influence on the photocatalytic activity of TiO_2 films prepared by micro-plasma oxidation method, J. Mol. Catal. A: Chem. 268 (2007) 257–263.